TESTING THE SERSIC BULGE – BLACK HOLE MASS RELATION IN SEYFERT GALAXIES

by

ALANA JADE MAY

A THESIS

Submitted in partial fulfillment of the requirements
for the degree of Master of Science
in the Department of Physics and Astronomy
in the Graduate School of
The University of Alabama

TUSCALOOSA, ALABAMA

2010

ABSTRACT

Using a sample of Active Galactic Nuclei (AGN), we investigated the relationship between host galaxy and black hole mass using the Sérsic index. We performed two-dimensional (2-D) decompositions of high-resolution Hubble Space Telescope images of (AGN) using GALFIT 3 beta. Taking independent mass estimates for a subsample of the selected galaxies, we test both linear and quadratic regressions in order to find an optimal relation for estimating black hole mass in other galaxies. Our results show that there was little difference between the linear and higher order fits. We examine the effects of these analysis techniques on the black hole mass to luminosity relationship. Application of the data was also considered concerning properties of pseudo- and classical bulges.

ACKNOWLEDGMENTS

Words cannot fully express how much I appreciate everyone for their contributions, both big and small. It has been a long journey to get to this point; one that would have been impossible without the love and support from so many people.

I thank my husband, Branyon, who never stopped encouraging me. He was my constant source of support and guidance, who unselfishly gave me his love and time.

I thank my daughters, Branna and Saige, who even though are too young to know, gave me knowledge beyond measure. Through them, I have gained a deeper appreciation of faith, love, and life.

I thank my parents, Andy and Katrina and Larry and Janis, and my family for standing behind me 100% of the time. They have seen me through the many years of my education and the successes and failures that go along with it.

I thank my advisor, William C. Keel who has imparted much knowledge and guidance. I am very grateful that he was willing to continue to work with me under less than ideal circumstances, namely being three states away.

I thank all my friends for their constant cheerleading and willingness to help me in so many ways. They were always there to listen and give a shoulder.

CONTENTS

LIST OF TABLES

LIST OF FIGURES

1. Introduction

A. Black Holes

For many decades, scientists theorized that massive compact objects existed at the center of galaxies (Salpeter, 1964; Rees, 1978). With the advent of bigger and better telescopes, especially those that are space-based, the theory of these massive compact objects has become reality, namely the black hole. By the late 1990's, it had been shown that almost every nearby galaxy was host to a black hole (Magorrian, et al., 1998).

Once it was discovered that nearly all galaxies harbored a central black hole, these objects became important in an effort to find out more about galactic formation. While there are many intriguing aspects to these anomalous objects and much that is yet to be discovered, there is a growing amount of scientific data leading us to the big picture of the Universe's structure and existence. One such example is the correlation between the host galaxy and black hole mass properties. It is thought that as a host galaxy becomes more massive, its black hole partner will in turn grow proportionally, leading to a supermassive black hole (SMBH; $M_{bh} \geq 10^6 M_{sun}$). Many parameters such as velocity dispersion, bulge luminosity, and the light concentration are thought to be linked to the co-formation of host galaxy and the black hole growth.

Currently, many factors seem to represent manifestations of the host galaxy-black hole inter-relationship. It is advantageous to breakdown the overall investigation into four parts: active or quiescent galaxies and nearby or distant galaxies. This study focuses on nearby, active, spiral galaxies, specifically Seyfert galaxies.

B. Seyfert Galaxies

Active Galactic Nuclei (AGN) are some of the most extreme power-houses, hosting some of the most luminous nuclei in the universe. A typical AGN produces anywhere from 10^{40} erg-s^{-1} to 10^{47} erg-s^{-1}. Since AGN produce such a massive amount of energy, it is believed that most, if not all, AGN are powered by SMBHs. Accretion of material is thought to be the driving force within these galaxies that feed the black hole (King, 2003).

Seyferts are an intermediate-luminosity (10^{43} erg-s^{-1} to 10^{45} erg-s^{-1}) subclass of AGN (Crenshaw, Kraemer, & Gabel, 2003). Accounting for only a fraction of giant galaxies, Seyferts release huge amounts of energy. In comparison to the number of stars in the galaxy, this energy is greater than what it should be (Halliday, 1969; Osterbrock, 1984). This energy generation has prompted astronomers to investigate the mechanism of what controls the AGN and find clues to how it fits our understanding of the universe.

Seyfert galaxies were the perfect candidate for the project since they are active galaxies that are each thought to host massive black holes. While this paper does not study the mechanism behind black hole growth, it does seek to further investigate the relationship between host galaxy (specifically the concentration of stars within the bulge) and black hole for active nearby galaxies.

C. Black Holes vs. Host Galaxy

Black hole masses can be predicted by several host galaxy characteristics including stellar velocity dispersion, bulge luminosity, bulge mass, and the measure of concentration of stars within the bulge (Sérsic index, n). Based on current research, AGN have been shown to roughly follow the same black hole mass (M_{bh}) to stellar velocity dispersion (σ_*) and bulge luminosity (L_{bul}) relation as inactive galaxies (Greene & Ho, 2006; Marconi & Hunt, 2003). Probably the

most widely used method is the relation between mass and stellar velocity dispersion, or M_{bh}–σ_*, relation. This is due to its good correlation and small level of scatter (Ferrarese & Merritt, 2000).

The Sérsic profile is defined by the equation:

$$I(R) = I_e \exp\{-b_n[(\frac{R}{R_e})^{1/n}-1]\} \quad (1)$$

where I_e is the intensity at the effective radius, R_e (the radius that contains half of the total light), and n a dimensionless index that measures the curvature of the luminosity profile (Sérsic, 1963). The M_{bh} -Sérsic index relation has an equivalent level of scatter as the M_{bh}-σ_* relation, as well as several other advantages (Graham & Driver, 2007). Unlike the M_{bh}- σ_* relation where spectra are required, the Sérsic profile only needs galaxy images, which are not required to be photometrically calibrated. Additionally, n is not heavily affected by the possibility of kinematical substructures at the center of a bulge. Nor is it affected by an underlying disk's rotational velocity or velocity dispersion or by aperture corrections. Other advantageous properties of the quantity n are that it doesn't depend on galaxy distance (as long as the bulge is well resolved) or an uncertain mass-to-light ratio.

2. The Sample

A. Our Sample

Keeping the advantageous properties of the Sérsic index in mind, we modeled images taken with the Hubble Space Telescope (HST) via GALFIT 3 beta, a 2-D image fitting algorithm for galaxy analysis (Peng, Ho, Impey, & Rix, 2010). After the galaxy was modeled by GALFIT, the Sérsic index of the bulge was taken and used to obtain a relationship that could be extended to calculate the black hole mass of a galaxy. Because the focus of this project was examining nearby AGN, a preselected group of 256 galaxies was taken from a study by Malkan, Gorjian, & Tam (1998). Malkan et al. selected the sample of AGN from the Veron-Cetty & Veron (VCV) Catalog of Quasars and Active Nuclei having criteria of $z \leq 0.035$ and not to be duplicated by other cycle 4 HST observing programs. Galaxies were imaged with a uniform exposure time (500 seconds) and filter (Wide Field Planetary Camera 2 F606W). From this sample, we chose Seyfert galaxies that were symmetric and that fit into the Wide Field Planetary Camera 2 (WFPC2) field of view. In 2006, The University of Alabama had the opportunity to join the Southeastern Association for Research Astronomy (SARA). Taking advantage of access to the 0.9 meter telescope, images of 11 galaxies that were bigger than the WFPC2 field of view were taken and added to the sample. Of the remaining galaxies, 37 would not converge to a sufficient model in GALFIT because of faint spiral structure and star-forming knots. Taking these constraints into account, left 72 galaxies for our sample. These galaxies and their properties are given in Table 1.

Table 1
Galaxy Parameters

TargetName (1)	SeyfertClass (2)	z (3)	D(Mpc) (4)	Log(M_{bh}) (5)	References (6)
ESO323-G77	1	0.015	62	7.39	c
ESO362-G18	1	0.013	54	7.49	c
F1146	1	0.032	133	7.83	c
F294	2	0.017	71	----	-
F341	2	0.016	67	----	-
HEAO-1-0307-730	1	0.028	117	7.35	c
IC184	2	0.018	75	----	-
IR0147-076	2	0.017	71	7.55	c
IR0258-1136	2	0.030	125	----	-
IR0450-032	2	0.016	67	----	-
IR1121-281	2	0.014	58	----	-
IR1443+272	2	0.029	121	----	-
IR1548-037	2	0.030	125	8.22	c
IR1832-594	2	0.019	79	----	-
IR2346+019	2	0.031	129	----	-
MCG8-11-11*	1	0.030	125	7.89	c
MARK1	2	0.016	67	6.21	b
MARK1058	2	0.018	75	----	-
MARK1193	2	0.032	133	----	-
MARK1210	2	0.013	54	6.29	b
MARK1218	1	0.028	117	----	-
MARK1330*	1	0.009	37	7.22	c
MARK1370	2	0.024	100	----	-
MARK1400	1	0.029	121	----	-
MARK1469	1	0.031	129	7.49	a
MARK198	2	0.024	100	----	-
MARK279	1	0.031	129	7.92	c
MARK290	1	0.029	121	7.65	c
MARK335	1	0.025	104	----	-
MARK352	1	0.015	62	6.65	c
MARK372	1	0.031	129	7.34	c
MARK40	1	0.020	83	7.47	c
MARK403	2	0.024	100	7.24	a
MARK42	1	0.024	100	----	-
MARK423	1	0.032	133	----	-
MARK50	1	0.023	96	6.29	a
MARK543	1	0.026	108	7.57	c
MARK595	1	0.028	117	7.38	c
MARK6	1	0.019	79	8.29	c
MARK609	1	0.032	133	----	-
MARK612	2	0.020	83	----	-
MARK699	1	0.034	142	----	-
MARK79*	1	0.022	92	7.98	c
MARK744*	1	0.01	42	----	-
MARK817	1	0.033	108	----	-

MARK917	2	0.025	104	----	-
MS1110+2210	1	0.030	125	----	-
NGC1410	2	0.025	104	----	-
NGC235	1	0.022	92	----	-
NGC2110*	2	0.007	29	----	-
NGC2639*	1	0.011	46	7.61	b
NGC2992*	2	0.007	29	----	-
NGC4235*	1	0.007	29	7.88	c
NGC4922B	2	0.024	100	----	-
NGC4939*	2	0.010	42	----	-
NGC513	2	0.016	67	7.61	a
NGC5252	1	0.022	92	----	-
NGC526A	1	0.018	75	8.33	b
NGC5674*	1	0.025	104	----	-
NGC6211	2	0.020	83	8.39	a
NGC6212	1	0.030	125	7.34	c
PKS0518-458	1	0.034	142	----	-
PKS2158-380	2	0.033	137	----	-
TOL1059+105	1	0.034	142	----	-
UGC10683B	1	0.031	129	7.66	c
UGC6100*	2	0.029	121	----	-
UM614	1	0.033	137	7.49	a
UM625	2	0.025	104	----	-
WAS2	2	0.033	137	----	-
X0459+034	1	0.016	67	----	-
ZW1541+286	2	0.032	133	----	-

Note- (1) object name;(2) Seyfert classification;(3) redshift;(4) distance; (5) black hole mass from literature search; (6) reference for columns (5). Columns (1), (2), and (3) are taken from Malkan et al. (1998)
** indicates galaxy taken with SARA telescope*
References- (a) HYPERLEDA, Paturel, et al., 2003;(b)Garcia-Rissmann, et al., 2005);(c)Wang & Zhang, 2007

B. Data Analysis

We retrieved images of the galaxies through the HST Archival search. Upon retrieval, each galaxy was pieced together using IRAF's `wfpc` package and `wmosaic` commands. After the image was recreated, cosmic rays were median filtered and the sky background was subtracted. This subtracted image is the image used in the GALFIT modeling.

Images taken with the SARA telescope were taken with V and R filters. Using sample galaxy spectra, we found that a good predictor of flux in the F606W filter was an equal combination of

V and R images. These images were cleaned using typical IRAF techniques. The galaxies were then rotated and shifted to match their HST image counterpart. In order to recreate the SARA image and roughly match resolutions, the HST image was convolved with a Gaussian. A pixel-by-pixel least-squares linear fit yielded the relative count rates of the SARA and HST images. From this, the sky brightness was found and subtracted from the HST image for these galaxies which filled the WFPC2 field of view.

Basic starting parameters for each galaxy, such as galactic center, disk scale length, and half-light radius were manually measured from the HST images. These parameters were put into the appropriate GALFIT template.

A bulge-disk decomposition was attempted for each galaxy using GALFIT 3's ability to simultaneously fit multiple galaxy components. For the majority of the sample, a small Sérsic was used to account for the contribution of the bright nucleus, simulating a point-spread-function (PSF).

Typically, the exponential disk template was run first in order establish a model of the galaxy's spiral arms. GALFIT 3 uses the term exponential disk in the historical form, in the sense that one may be modeling a classical disk with a scale length r_s. (This does not necessarily have to be the case since the exponential disk is a special case of the Sérsic function for n=1.) The 6 free parameters of the exponential profile are: the center positions x and y, the integrated magnitude (m_{tot}), disk scale length (r_s), axis ratio (q), and position angle (Θ_{PA}).

Fourier modes were added to the disk component as needed to create the details of the spiral structure. The number of modes is defined by N and is determined by the user. GALFIT 3 creates spiral structure by a hyperbolic tangent rotation function with the following parameters: bar radius, spiral outer radius, rotation rate, sky inclination, and sky position angle.

After the disk was sufficiently modeled, the Sérsic functions for the bulge and nuclear regions were added and allowed to run. The Sérsic functions were run with 7 classical parameters: the center positions x and y, the integrated magnitude (m_{tot}), half-light radius (r_e), Sérsic index (n), axis ratio (q), and position angle (Θ_{PA}).

Listed in Table 2 are the galaxy properties derived from GALFIT 3. We show in Figure 1 five sample galaxies with the corresponding GALFIT 3 model and residual image.

Table 2
GALFIT Derived Galaxy Properties

TargetName (1)	Sersic Index (2)	$m_{,integrate,\ bulge}$ (3)	B/D (4)	$M_{V,\ bulge}$ (5)	Log(M_{bh}) (6)
ESO323-G77	2.45	-7.5	0.145	-18.44	7.57
ESO362-G18	3.35	-9.16	0.402	-19.79	7.83
F1146	4.45	-8.73	0.240	-21.32	8.15
F294	1.58	-9.18	3.945	-20.40	7.32
F341	1.94	-9.1	0.090	-20.18	7.42
HEAO-1-0307-730	1.59	-6.89	0.215	-19.19	7.32
IC184	1.69	-8.24	0.215	-19.58	7.35
IR0147-076	1.41	-6.31	----	-17.53	7.27
IR0258-1136	2.42	-8.69	0.847	-21.14	7.56
IR0450-032	1.47	-7.89	0.619	-18.97	7.29
IR1121-281	5.19	-8.05	----	-18.84	8.37
IR1443+272	0.51	-7.56	1.047	-19.94	7.01
IR1548-037	4.76	-8.12	0.158	-20.57	8.24
IR1832-594	1.64	-8.74	1.528	-20.20	7.34
IR2346+019	0.55	-8.37	1.690	-20.89	7.02
MCG8-11-11*	2.90	-10.50	0.80	-22.95	7.70
MARK1	1.31	-7.7	0.360	-18.78	7.24
MARK1058	0.72	-8.56	1.556	-19.90	7.07
MARK1193	0.28	-7.34	1.067	-19.93	6.94
MARK1210	0.37	-7.73	-0.47	-18.36	6.97
MARK1218	1.59	-8.78	1.706	-21.08	7.32
MARK1370	3.73	-8.19	----	-20.16	7.94
MARK1330*	2.50	-13.50	1.58	-23.34	7.59
MARK1400	2.88	-8.11	3.221	-20.49	7.70
MARK1469	1.72	-8.29	----	-20.81	7.36
MARK198	3.9	-8.86	4.786	-20.83	7.99
MARK290	3.59	-8.12	9.727	-20.50	7.90
MARK335	4.97	-7.42	----	-19.47	8.30
MARK352	0.79	-7.42	----	-18.36	7.09
MARK372	1.21	-8.5	1.837	-21.02	7.21
MARK40	2.95	-8.19	----	-19.76	7.72
MARK403	2.27	-8.46	1.067	-20.43	7.52
MARK42	1.47	-3.17	0.004	-15.14	7.29
MARK423	1.67	-8.27	1.923	-20.86	7.34
MARK50	1.83	-8.01	----	-19.88	7.39
MARK595	2.28	-8.43	----	-20.73	7.52
MARK6	3.94	-9.56	----	-21.02	8.00
MARK609	1.67	-7.83	0.325	-20.42	7.34
MARK612	3.65	-9.32	5.808	-20.89	7.92
MARK699	2.91	-7.84	----	-20.56	7.70
MARK79*	2.50	-13.50	1.58	-25.28	7.59
MARK744*	2.36	-8.77	0.05	-18.83	7.54
MARK817	0.49	-8.52	0.17	-20.66	7.00
MARK885	4.7	-4.71	0.012	-17.37	8.22

MARK917	1.33	-8.15	0.398	-20.20	7.25
MS1110+2210	2.63	-7.07	----	-19.52	7.62
NGC1410	1.9	-7.73	1.009	-19.78	7.41
NGC235	1.4	-8.24	0.373	-20.02	7.27
NGC2110*	2.24	-10.90	15.14	-20.19	7.51
NGC2639*	1.63	-11.01	0.90	-21.28	7.33
NGC2992*	2.12	-11.23	----	-20.52	7.47
NGC4922B	0.46	-8.94	----	-20.91	6.99
NGC4235*	1.48	-10.84	1.45	-20.13	7.29
NGC4939*	1.30	-11.39	1.13	-21.45	7.24
NGC513	1.84	-6.31	0.022	-17.39	7.39
NGC5252	3.9	-10.16	----	-21.94	7.99
NGC526A	3.81	-9.34	----	-20.68	7.96
NGC5674*	3.79	-9.89	1.32	-21.94	7.96
NGC6211	3.25	-10.42	----	-21.99	7.80
NGC6212	1.3	-7.8	0.316	-20.25	7.24
PKS0518-458	3.67	-7.84	----	-20.56	7.92
PKS2158-380	2.94	-9.2	11.912	-21.86	7.71
TOL1059+105	2.86	-7.05	----	-19.77	7.69
UGC10683B	2.55	-6.39	0.091	-18.91	7.60
UGC6100	2.23	-9.91	4.97	-22.29	7.51
UM614	1.11	-7.52	----	-20.18	7.18
UM625	5.15	-7.75	----	-19.80	8.35
WAS2	1.65	-8.39	0.124	-21.05	7.34
X0459+034	1.44	-8.28	----	-19.36	7.28
ZW1541+286	1.16	-7.3	0.802	-19.89	7.20

Note- (1) object name;(2) Sérsic index;(3)integrated magnitude of the bulge (F606W);(4) bulge-to-disk ratio;(5) absolute v-band magnitude;(6) estimated black hole mass from equation 2
** indicate galaxy taken with SARA telescope*

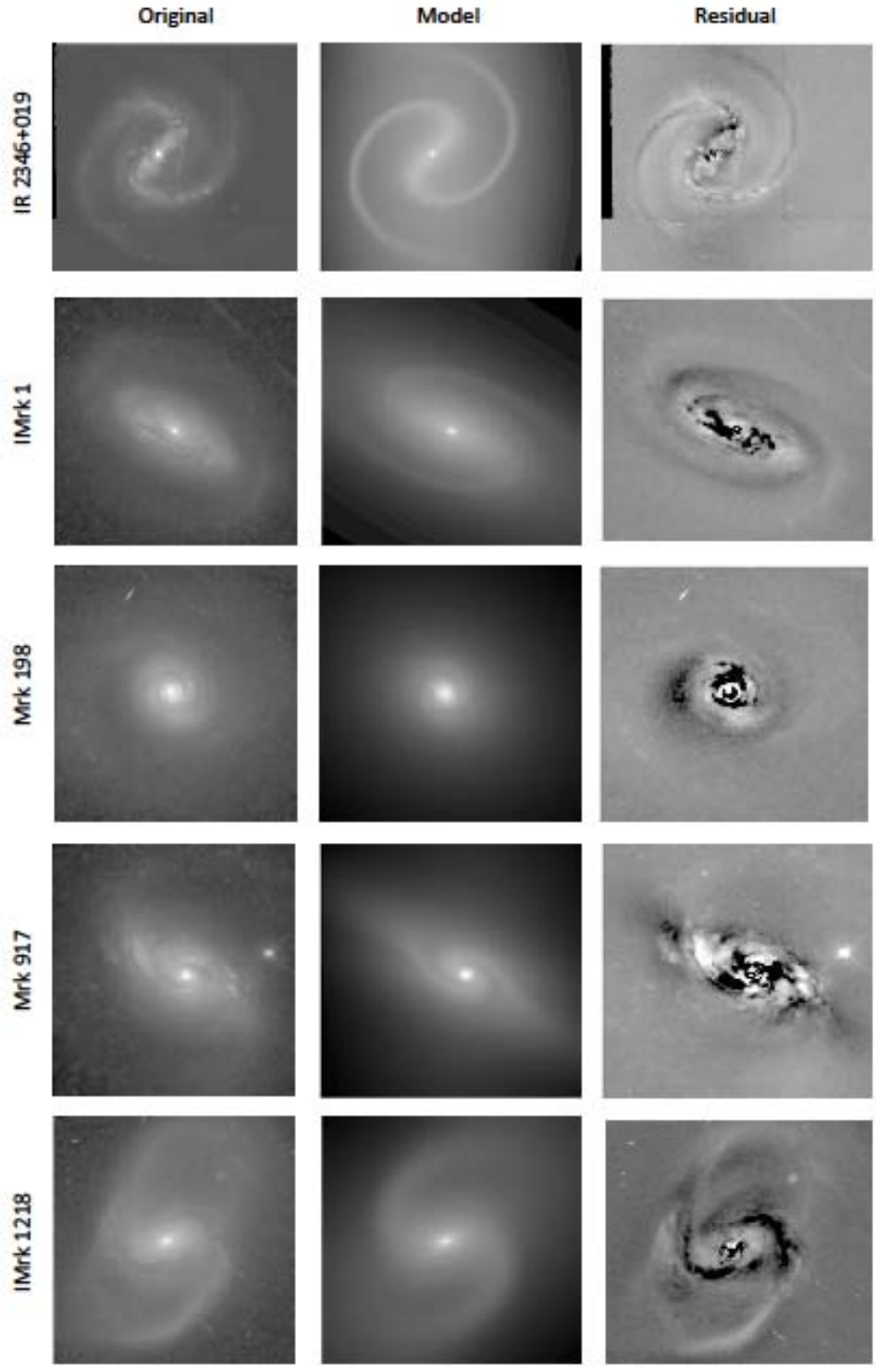

Figure 1. Examples of sample objects.
From left to right: original galaxy image, model, residual image.

3. The Sérsic Index Put to the Test

A. Our Sample

A data search for established black hole masses within our sample was carried out. While we found numerous mass estimates, it was often the case that only one or two measurements for the given sample could be taken from a particular reference. To ensure consistency, 3 references that provided the most data was used. They were: HYPERLEDA, Garcia-Rissmann et al. (2005), and Wang and Zhang, (2007). The first two sources base their estimates from stellar velocity dispersion measurements, while the latter uses H_β and OIII line width (thus measuring the velocity dispersion of the ionized gas). A comparison sample of 31 galaxies was taken from these 3 sources and given in Table 1.

To estimate M_{bh} via the Sérsic index, data were plotted with a typical x-y scatter. Using the established M_{bh} plotted against the Sérsic index, found via galaxy decomposition using GALFIT, a linear regression was performed, giving an equation of

$$\log(M_{bh}) = (0.29 \pm 0.07)\mathrm{n} + (6.85 \pm 0.18) \qquad (2)$$

Similarly, a quadratic regression was performed, giving the relation:

$$\log(M_{bh}) = (-0.011 \pm 0.06)n^2 + (0.35 \pm 0.31)\mathrm{n} + (6.80 \pm 0.35) \qquad (3)$$

Both fits had an R value of 0.6 and total scatter of 0.45 dex in $\log(M_{bh})$.

The trend lines for equations (2) and (3) were plotted and, looking at the data, these two relations are very similar to one another over the given range of values. Within the specified Sérsic range, there was no evidence for preferring the quadratic fit, implying no upper bound for this sample.

This is a significant difference from the Graham and Driver study (2007), where the quadratic gave a better fit.

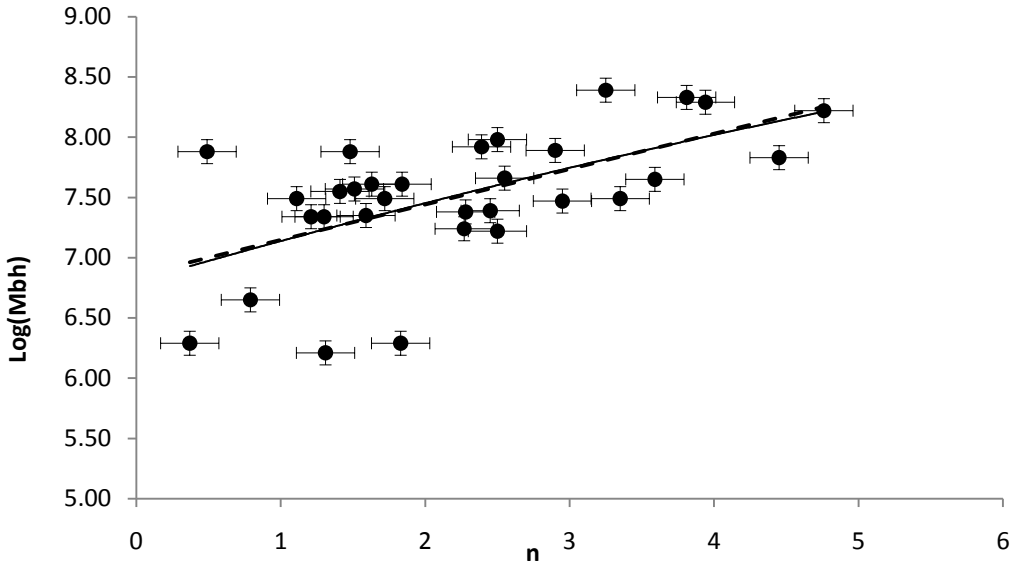

Figure 2. Established black hole masses vs. GALFIT derived Sérsic index
Correlation between the galaxy's supermassive black hole mass (established masses) and Sérsic index given by GALFIT 3. Linear equation (dashed line) is given by $log(M_{bh})= (0.29\pm0.07)n+(6.86\pm0.18)$. *Quadratic equation (solid line) is given by* $log(M_{bh})=(-0.011\pm0.06)n^2+(0.35\pm0.31)n+(6.80\pm0.35)$

B. The Graham and Driver Sample (2007)

In their paper, Graham and Driver (hereafter, GD07) set out to test the usefulness of the Sérsic index and how good of a predictor it would be in determining the black hole mass in other galaxies. From a sample of 27 galaxies with well establish black hole masses, GD07 performed a galaxy decomposition to obtain the Sérsic index for each galaxy. Using the known black hole masses and the Sérsic indices, a least-squares regression was carried out to obtain a suitable relationship. Taking an unbiased approach, they first tested the relationship with a linear regression and then tested it using a quadratic fit that accounted for apparent distribution curvature. Using a modified version of the Tremaine et al. (2002) FITEXY routine, they came up with a linear relationship of the form:

$$log(M_{bh}) = (2.69 \pm 0.28)\, log(\frac{n}{3}) + 7.81 \pm .08 \qquad (4)$$

having a total absolute scatter in log(M_{bh}) of 0.39 dex.

Graham and Driver then similarly performed a quadratic fit and obtained the following equation:

$$\log(M_{bh}) = (7.98 \pm 0.09) + (3.7 \pm 0.46)\log(\frac{n}{3}) - (3.10 \pm .084)[\log(\frac{n}{3})]^2 \qquad (5)$$

Comparing equations (4) and (5) it was found that the quadratic fit was better, since it was able to account for a wider range of masses than the linear relationship and also had a lower absolute scatter, ~0.31 dex.

Because of the intrinsic nature of the quadratic function, there will be an upper-end and a lower-end to the mass function. The maximum mass can be found when the derivative of the given relationship equals zero. For GD07, this is

$$\frac{dM_{bh}}{d\log(\frac{n}{3})} = 2cx + b = 2(-3.10)\log\left(\frac{n}{3}\right) + 3.70 = 0 \qquad (6)$$

The turnover point occurs when n=11.9 and corresponds to a SMBH of 1.2×10^9 M_{sun}.

C.Discussion

Referring back to GD07's data, 3 galaxies showed extreme Sérsic indices, falling above their maximum (n=11.9) in the quadratic fit. When it was investigated further, these specific galaxies turned out to be 2 ellipticals and one spiral. If we reevaluate the GD07 data and exclude the 3 galaxies with extreme Sérsic indices, their quadratic relation is substantially altered and there is less significance to the difference between a linear fit (equation 7) and quadratic fit (equation 8).

$$\log(M_{bh}) = (0.41 \pm 0.04)n + (6.50 \pm 0.17) \qquad (7)$$

$$\log(M_{bh}) = (-0.057 \pm 0.02)n^2 + (0.88 \pm 0.19)n + (5.73 \pm 0.34) \qquad (8)$$

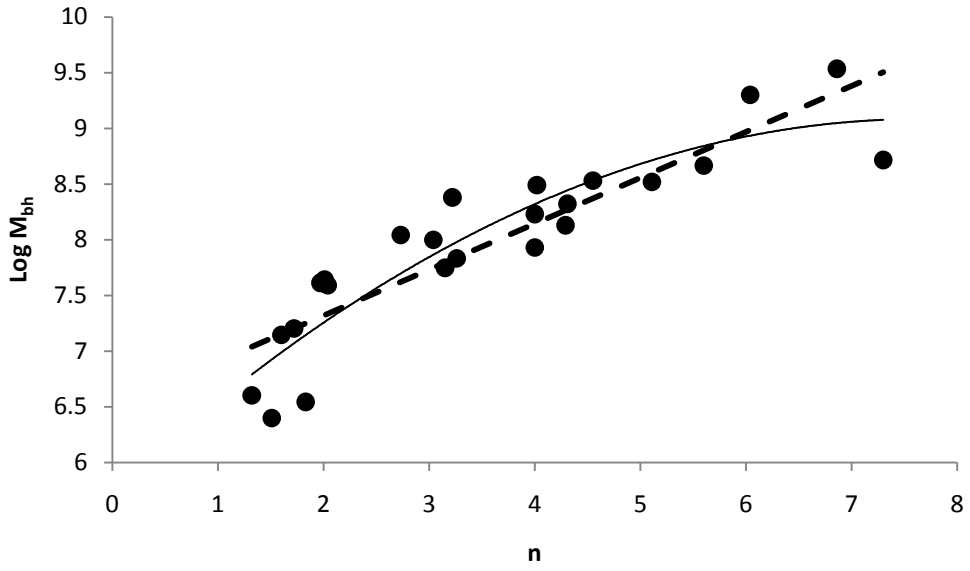

Figure 3. Graham and Driver black hole masses vs. Sérsic index
Correlation of Graham and Drivers's black hole mass to Sérsic index with the 3 extreme Sérsic indices excluded . As in the previous figure, the linear fit is represented by the dashed line and the quadratic fit is represented by the solid line.

It is of interest to note that the S0 galaxy, NGC3115, might have an overly large Sérsic index. Based on GD07, its Sérsic index is n= 13 and has a listed mass of M_{bh}=9.2x10^8. Hu (2008) also studied the galaxy NGC3115 and give a reference of n=4.4 and mass of M_{bh} =1x10^9.

Hu gives a table comparison of 44 previously referenced black hole masses and the corresponding Sérsic indices. These data have a similar range of black hole masses (10^6-10^9 M_{sun}) and Sérsic indices (n≈1-7) as the data of this paper. Taking Hu's referenced data, points were plotted on an x-y scatter and a linear regression was performed in a similar manner. Respectively, the linear equation and quadratic equations are:

$$\log(M_{bh}) = (0.37 \pm 0.06)n + (6.77 \pm 0.23) \quad (9)$$

$$\log(M_{bh}) = (-0.0057 \pm 0.04)n^2 + (0.41 \pm 0.25)n + (6.71 \pm 0.43) \quad (10)$$

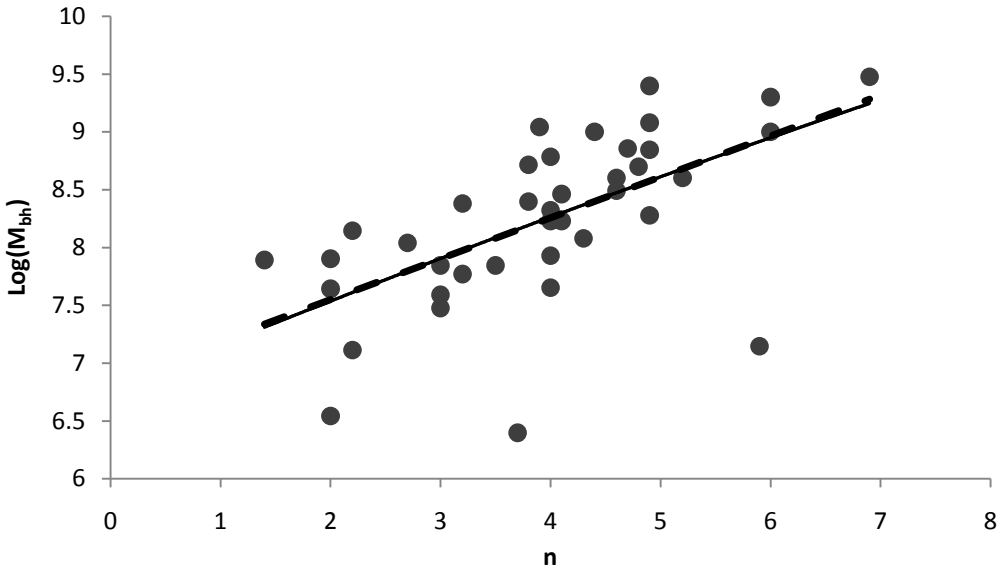

Figure 4. Hu black hole mass vs. Sérsic index
Correlation of Hu (2008)M_{bh} and Sérsic index As in previous figures, the linear equation is denoted by the dashed line and the quadratic equation is denoted by the solid line.

Both fits had an R value of 0.7 and total scatter of 0.56 dex in log(M_{bh}). These relationships are very similar to equations (2) and (3), where both the slope and intercept coefficients fall within the error bars of our estimates.

4. Luminosity

As mentioned in the Data Analysis section, one of the resulting galaxy parameters from the Sérsic function in GALFIT 3 is the integrated magnitude. Since the Malkan et al. (1998) observations use the WFPC2 camera and the F606W filter, the resulting integrated magnitude is from the same filter. In order to transform to the common Johnson V-band magnitudes, we used the transformation and corresponding zero points described in Holtzman et al. (1995). From this, the absolute magnitude of the bulge component was calculated using the following equations:

$$m_{V,bulge} = 22.83 + 0.254 \times 0.8 + m_{Integrated\ \ Magnitude} \quad (11)$$

$$\mathrm{M_{V,bulge}} = \mathrm{m_{v,bulge}} - 5 \times \log(\mathrm{D_{Mpc}} \times 10^5) \quad (12)$$

where distance ($\mathrm{D_{Mpc}}$) is calculated from redshift given in Table 1. It is noted that using redshifts alone to infer distance gives a potential source of error that becomes less important with increasing redshift. In Figure 5, the estimated black hole mass against the absolute V-band magnitude of the bulge is plotted. Our sample (plotted as circles) shows the typical relation of increasing black hole mass with increasing luminosity. Kim et al. (2008) also use GALFIT to obtain bulge luminosities for quasars and Seyfert 1 galaxies, where the black hole masses are derived from reverberation mapping and single-epoch emission-line spectra. Their higher-redshift, higher-luminosity data (represented by crosses) extends our current low-redshift, low-luminosity sample well.

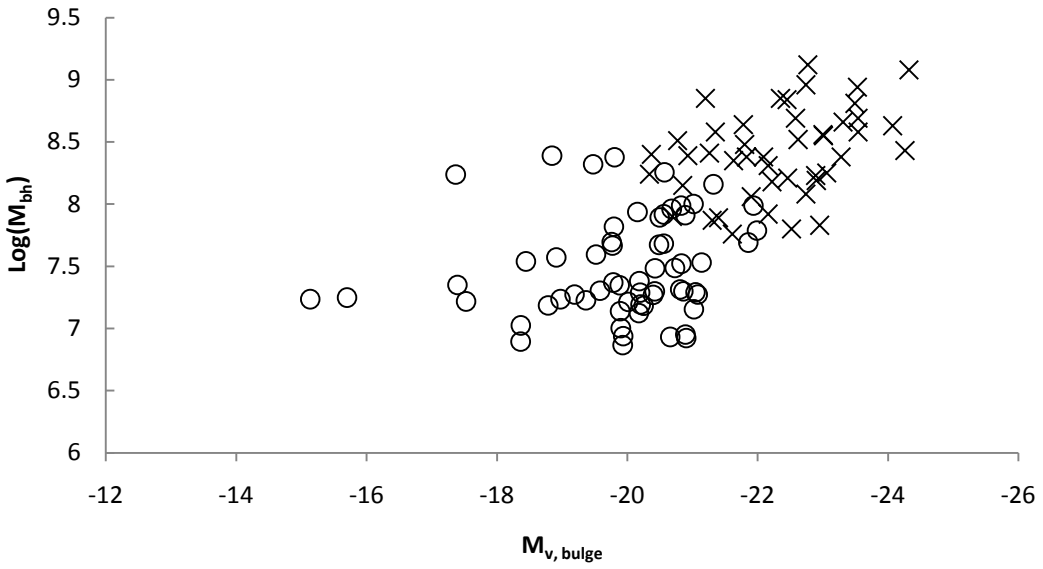

Figure 5. Black hole mass vs. bulge luminosity
Correlation of the luminosity of the bulge and black hole mass. Kim et al. (2008) data are represented by crosses and our sample by circles.

5. Pseudobulge vs. Classical Bulge

It has been established that there are two types of bulges: classical bulges and pseudobulges. Classical bulges are dynamically hot systems and have morphologies that resemble elliptical galaxies, but happen to have a disk around them. Pseudobulges, on the other hand, are bulges that have kinematics resembling a disk and internal structure. Examples of internal structure include nuclear bars, nuclear disks, nuclear spiral structure, boxy bulges, exponential bulges, and central star formation (Kormendy & Kennicutt, 2004). Pseudobulges are dynamically cold and have flattening similar to the outer disk.

Another distinguishing factor between the classical bulge and pseudobulge is the Sérsic index. In a 2008 paper, Fisher & Drory examine this relationship. Their study shows that the Sérsic index can indeed discriminate between pseudobulges and classical bulges. No classical bulge has a Sérsic index less than two and very few (~10%) pseudobulges have Sérsic index greater than 2. For the purposes of this paper, we adopt the convention of the division: a classical bulge is defined by $n>2$ and a pseudobulge is defined by $n<2$.

This relationship can help to improve our understanding of the bulge. The uniqueness and availability of the Sérsic index allows for one to easily distinguish between a classical bulge or pseudobulge without the need for high resolution images or kinematical data. It can also help to constrain current formation models.

Based on the Sérsic index criteria, our sample was equally divided with 47% of the galaxies being pseudobulges and 53% being classical bulges. Seyfert 1 galaxies account for 57% of the total galaxies. Two galaxies (NGC4922 and NGC1410 both with $n<2$) are left out of this

comparison sample because they are interacting galaxies. With the presence of a companion, it cannot be clearly ruled out that the pseudobulge is not an artifact of the merger. (Drory & Fisher, 2007). Of the pseudobulges, 51% were Seyfert 1 galaxies, which was slightly below the full sample and 62% of the classical bulges were Seyfert 1, which was slightly above the full sample. On average, pseudobulges tend to have a lower luminosity than classical bulges. In Fisher and Drory's 2008 sample, they find that pseudobulges are ~1.2 magnitudes fainter than classical bulges. Our sample exhibits a similar trend with the average pseudobulge being 0.9 magnitudes fainter, as shown in Figure 6.

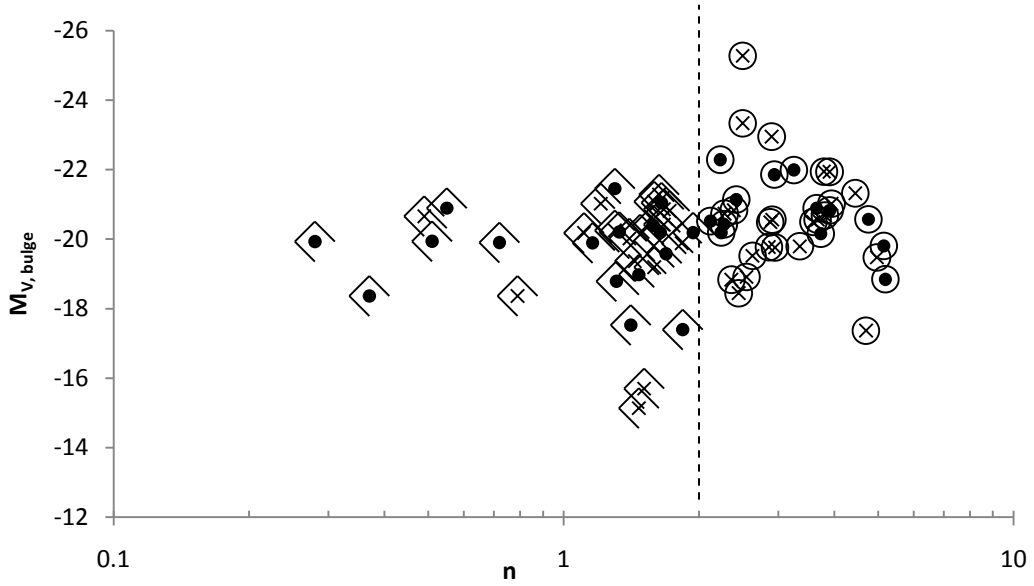

Figure 6. Black hole mass vs. absolute luminosity
Absolute magnitude plotted against log(n) for pseudobulges (diamonds) and classical bulges (circles). Seyfert 1s are denoted by crosses and Seyfert 2s by closed circles. Dashed line marks the pseudobulge/classical bulge division.

Drory and Fisher (2008) investigate the possible relationship between the bulge-to-total luminosity ratio and the half-light radius (r_e) to disk scale length (r_s) against the Sérsic index. They note that in their sample, there is an absence of correlation in both for pseudobulges,

possibly indicating that their formation could be non-merger driven. However, these results are only suggestive. Comparing our sample to the Drory-Fisher sample, a similarly large spread in the bulge-to-disk ratio (Figure7) and r_e/r_s (Figure 8) to Sérsic was present.

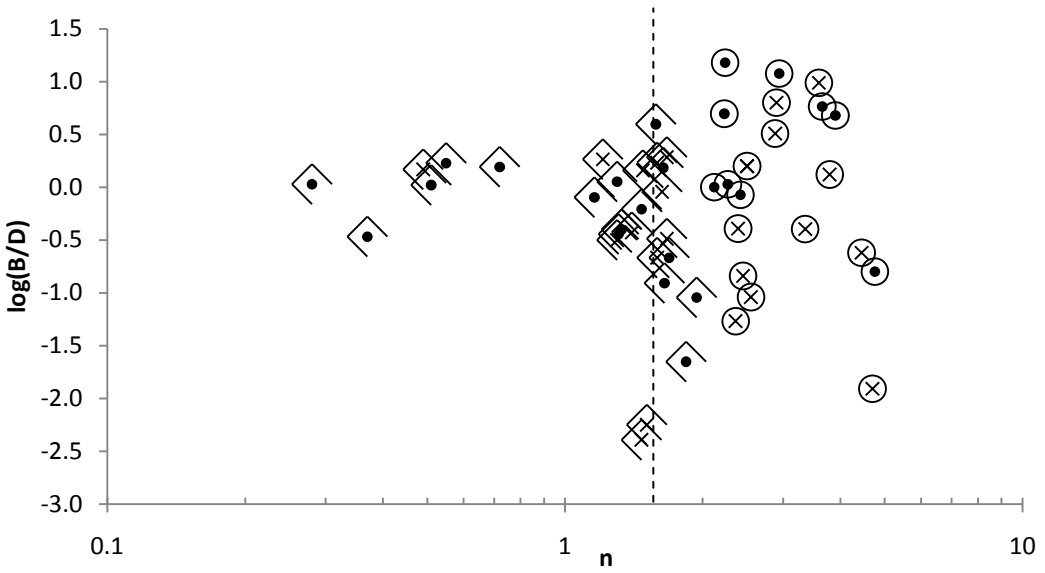

Figure 7. Bulge-to-disk ratio vs. GALFIT derived Sérsic index
Bulge-to-disk ratio plotted against log(n) for pseudobulges (diamonds) and classical bulges (circles). Seyfert 1s are denoted by crosses and Seyfert 2s by closed circles. Dashed line marks the pseudobulge/classical bulge division.

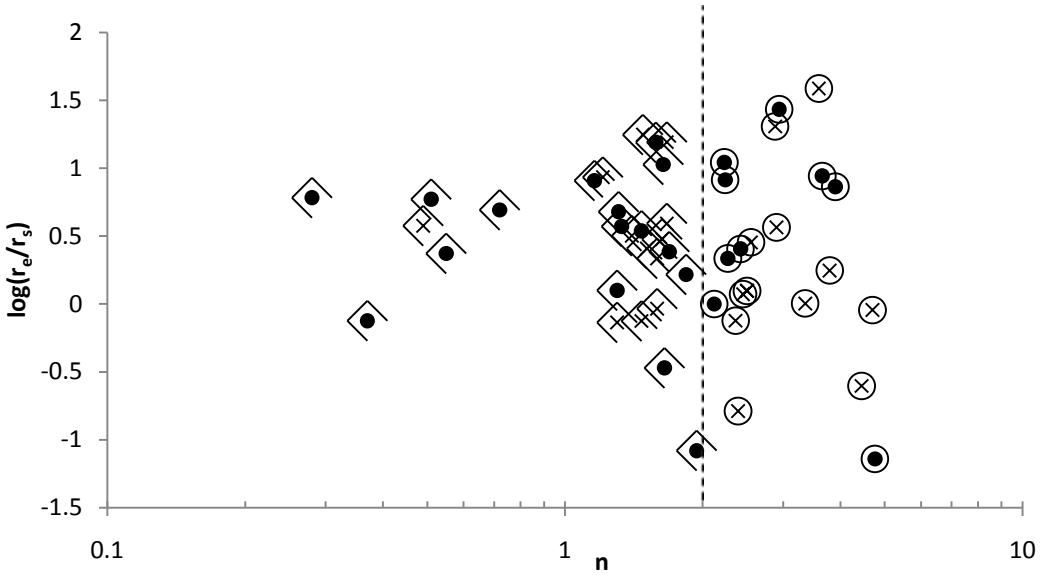

Figure 8. Ratio of half'light radius to disk scale length vs. GALFIT derived Sérsic index
Ratio of half'light radius (r_e) to disk scale length (r_s) plotted against log(n) for pseudobulges (diamonds) and classical bulges (circles). Seyfert 1s are denoted by crosses and Seyfert 2s by closed circles. Dashed line marks the pseudobulge/classical bulge division.

6. Conclusions

Investigating the correlations between host galaxy and black hole mass is important in understanding the structure of the Universe. We have presented new data that helps strengthen this investigation. A linear relation [$\log(M_{bh})= (0.29\pm0.07)n+(6.86\pm0.18)$] to estimate black hole mass using the Sérsic index was determined and is consistent with other data. Using galaxy properties derived from GALFIT 3, the relationship between black hole mass and luminosity was found to reflect the accepted linear trend. Our data was also applied to the current understanding of pseudobulges and classical bulges. As predicted, the pseudobulges in our sample had lower luminosity (~0.9 magnitudes) than classical bulges. Our sample also found no correlation between Sérsic index with B/D and r_e/ r_s in pseudobulges.

References

Crenshaw, D. M., Kraemer, S. B., & Gabel, J. R. (2003). The Host Galaxies of Narrow-Line Seyfert 1 Galaxies: Evidence for Bar-Driven Fueling. *The Astronomical Journal, Volume 126, Issue 4* , 1690-1698.

Drory, N., & Fisher, D. B. (2007). A Connection between Bulge Properties and the Bimodality of Galaxies. *The Astrophysical Journal, Volume 664, Issue 2* , 640-649.

Ferrarese, L., & Merritt, D. (2000). A Fundamental Relation between Supermassive Black Holes and Their Host Galaxies. *The Astrophysical Journal, Volume 539, Issue 1* , L9-L12.

Fisher, D. B., & Drory, N. (2008). The Structure of Classical Bulges and Pseudobulges: the Link Between Pseudobulges and SÉRSIC Index. *The Astronomical Journal, Volume 136, Issue 2* , 773-839.

Garcia-Rissmann, A., Vega, L. R., Asari, N. V., Cid Fernandes, R., Schmitt, H., González Delgado, R. M., et al. (2005). An atlas of calcium triplet spectra of active galaxies. *Monthly Notices of the Royal Astronomical Society, Volume 359, Issue 2* , 765-780.

Graham, A. W. (2007). A Log-Quadratic Relation for Predicting Supermassive Black Hole Masses from the Host Bulge Sérsic Index. *The Astrophysical Journal, Volume 655, Issue 1* , 77-87.

Greene, J. E., & Ho, L. C. (2006). The Mbh- σ∗ Relation In Local Active Galaxies. *The Astrophysical Journal, Volume 641, Issue 1* , L21-L24.

Greene, J. E., Ho, L. C., & Barth, A. J. (2008). Black Holes in Pseudobulges and Spheroidals: A Change in the Black Hole-Bulge Scaling Relations at Low Mass. *The Astrophysical Journal, Volume 688, Issue 1* , 159-179.

Halliday, I. (1969). Advances in Astronomy Seyfert Galaxies and Quasars. *Journal of the Royal Astronomical Society of Canada, Vol. 63* , 91.

Holtzman, J. A., Burrows, C. J., Casertano, S., Hester, J. J., Trauger, J. T., Watson, A. M., et al. (1995). The Photometric Performance and Calibration of WFPC2. *Publications of the Astronomical Society of the Pacific, v.107* , 1065.

Hu, J. (2008). The black hole mass-stellar velocity dispersion correlation: bulges versus pseudo-bulges. *Monthly Notices of the Royal Astronomical Society, Volume 386, Issue 4* , 2242-2252.

Kim, M., Ho, L. C., Peng, C. Y., Barth, A. J., Im, M., Martini, P., et al. (2008). The Origin of the Intrinsic Scatter in the Relation Between Black Hole Mass and Bulge Luminosity for Nearby Active Galaxies. *The Astrophysical Journal, Volume 687, Issue 2* , 767-827.

King, A. (2003). Black Holes, Galaxy Formation, and the MBH-σ Relation. *The Astrophysical Journal, Volume 596, Issue 1* , L27-L29.

Kormendy, J., & Kennicutt, R. C. (2004). Secular Evolution and the Formation of Pseudobulges in Disk Galaxies. *Annual Review of Astronomy &Astrophysics, vol. 42, Issue 1* , 603-683.

Magorrian, J., Tremaine, S., Richstone, D., Bender, R., Bower, G., Dressler, A., et al. (1998). The Demography of Massive Dark Objects in Galaxy Centers. *The Astronomical Journal, Volume 115, Issue 6* , 2285-2305.

Malkan, M. A., Gorjian, V., & Tam, R. (1998). A Hubble Space Telescope Imaging Survey of Nearby Active Galactic Nuclei. *Astrophysical Journal Supplement v.117* , 25.

Marconi, A., & Hunt, L. K. (2003). The Relation between Black Hole Mass, Bulge Mass, and Near-Infrared Luminosity. *The Astrophysical Journal, Volume 589, Issue 1* , L21-L24.

Osterbrock, D. E. (1984). Active Galactic Nuclei. *Royal Astronomical Society Quarterly Journal, V. 25, No. 1* , 1.

Paturel, G., Petit, C., Prugniel, P., Theureau, G., Rousseau, J., Brouty, M., et al. (2003). HYPERLEDA. I. Identification and designation of galaxies. *Astronomy and Astrophysics, v.412* , 45-55.

Peng, C. Y., Ho, L. C., Impey, C. D., & Rix, H.-W. (2010). Detailed Decomposition of Galaxy Images. II. Beyond Axisymmetric Models. *Astrophysical Journal, 2009arXiv0912.0731P* .

Peng, C. Y., Ho, L. C., Impey, C. D., & Rix, H.-W. (2002). Detailed Structural Decomposition of Galaxy Images. *The Astronomical Journal, Volume 124, Issue 1* , 266-293.

Rees, M. J. (1978). Emission from the nuclei of nearby galaxies - Evidence for massive black holes. *Structure and properties of nearby galaxies; Proceedings of the Symposium* (pp. 237-244). Bad Muenstereifel, West Germany: Dordrecht, D. Reidel Publishing Co.

Salpeter, E. (1964). Accretion of Interstellar Matter by Massive Objects. *Astrophysical Journal, vol. 140* , 796-800.

Sérsic, J. (1963). Influence of the atmospheric and instrumental dispersion on the brightness distribution in a galaxy. *Boletin de la Asociacion Argentina de Astronomia, Vol. 6* , 41.

Tremaine, S., Gebhardt, K., Bender, R., Bower, G., Dressler, A., Faber, S. M., et al. (2002). The Slope of the Black Hole Mass versus Velocity Dispersion Correlation. *The Astrophysical Journal, Volume 574, Issue 2* , 740-753.

Wang, J.-M., & Zhang, E.-P. (2007). The Unified Model of Active Galactic Nuclei. II. Evolutionary Connection. *The Astrophysical Journal, Volume 660, Issue 2* , 1072-1092.